


RESEARCH ARTICLE

# Research and experiment on active training of lower limb based on five-bar mechanism of man-machine integration system

Jianghong Sun<sup>1,2</sup>, Fuqing Hu<sup>1</sup> , Keke Gao<sup>1</sup>, Feng Gao<sup>1</sup>, Chao Ma<sup>3</sup> and Junjian Wang<sup>4</sup>

<sup>1</sup>School of Mechanical Electrical Engineering, Beijing Information Science & Technology University, Beijing, PR China, <sup>2</sup>Institute of Mechatronic Engineering, Tsinghua University, Beijing, PR China, <sup>3</sup>Key Laboratory of Modern Measurement and Control Technology, Ministry of Education, Beijing Information Science and Technology University, Beijing, PR China, and <sup>4</sup>China National Machine Tool Quality Supervision Testing Center, Beijing, PR China

**Corresponding author:** Jianghong Sun; Email: [19960207@bistu.edu.cn](mailto:19960207@bistu.edu.cn)

**Received:** 14 September 2023; **Revised:** 23 December 2023; **Accepted:** 8 February 2024;

**First published online:** 14 March 2024

**Keywords:** lower limb active training; man-machine integration system; five-bar mechanism; forward and inverse kinematics; joint angle experiment

## Abstract

In view of the fact that the current research on active and passive rehabilitation training of lower limbs is mainly based on the analysis of exoskeleton prototype and the lack of analysis of the actual movement law of limbs, the human-machine coupling dynamic characteristics for active rehabilitation training of lower limbs are studied. In this paper, the forward and inverse kinematics are solved on the basis of innovatively integrating the lower limb and rehabilitation prototype into a human-machine integration system and equivalent to a five-bar mechanism. According to the constraint relationship of hip joint, knee joint and ankle joint, the Lagrange dynamic equation and simulation model of five-bar mechanism under the constraint of human physiological joint motion are constructed, and the simulation problem of closed-loop five-bar mechanism is solved. The joint angle experimental system was built to carry out rehabilitation training experiments to analyze the relationship between lower limb error and height, weight and BMI, and then, a personalized training planning method suitable for people with different lower limb sizes was proposed. The reliability of the method is proved by experiments. Therefore, we can obtain the law of limb movement on the basis of traditional rehabilitation training, appropriately reduce the training speed or reduce the man-machine position distance and reduce the training speed or increase the man-machine distance to reduce the error to obtain the range of motion angle closer to the theory of hip joint and knee joint respectively, so as to achieve better rehabilitation.

## 1. Introduction

In recent years, stroke hazards have become more and more obvious with the acceleration of population aging [1]. In 2019, it was nearly 1.74 million people in China have been plagued by stroke hazards, and the number of patients with limb movement disorders has surged, which causing 1.6 million annual deaths [2, 3]. Therefore, solving the problem of limb movement disorders has become a top priority [4–6].

Rehabilitation training in limb movement disorders is mainly aimed at the corresponding joints of the diseased limb, maintaining the muscle activity in active or passive way. According to the theory of brain plasticity, the structure and function of the nervous system can be reorganized and regenerated after a certain period of rehabilitation training [7]. Therefore, the effective rehabilitation training can improve nerve defects and develop the strength of muscle tissue and ultimately improve the degree of limb rehabilitation. Compared with traditional treatment methods, which maintain the activity of lower limb muscle tissue through patient's own walking training, the rehabilitation process of this method

is slow and lacks personalized treatment. Therefore, in order to improve the effect and quality of limb rehabilitation, it is urgent to explore more advanced and effective rehabilitation method [7, 8]. It reduces extremely the physical labor of rehabilitation doctors and monitors the data of limb rehabilitation training in real time, which can liberate manpower and make up for the shortage of manpower. Meanwhile, it is also providing a better choice for rehabilitation doctors to analyze the effects of therapeutic and optimize the treatment plan. Consequently, clinical rehabilitation training combined with limb rehabilitation robot technology has become a research hotspot at home and abroad [9].

Limb rehabilitation robot integrates mechatronics technology, robot technology, rehabilitation medicine and sensor technology into active and passive rehabilitation training of limbs [10–12]. Domestic and foreign scholars have carried out relevant research. Mohamed et al. [13] analyzed the dynamics of an electric-driven end-effector rehabilitation robot based on the Euler-Lagrangian principle and then designed an adaptive tracking control strategy under passive training, verifying the effectiveness of control strategy on experiments in different scenarios. Wang et al. [14] designed a 4DOF passive training rehabilitation robot for the lower limb, and the forward and inverse kinematics of the human-machine hybrid model was solved by D-H (Denav-Hartenberg) method, and then, a variable human-machine workspace based on the user was obtained, which shows that the rehabilitation robot can realize passive training of lower limb. Li et al. [15] conducted the dynamic analysis and parameter optimization under passive training by establishing the human-machine coupling dynamic model of lower limb rehabilitation robot system, the error of joint angle measured in the experiment was about 9%, which is verified the correctness of the dynamic model and the feasibility of the human-machine model for the rehabilitation training analysis. Ma et al. [16] collected human walking signal based on inertial measurement unit, established the motion model of lower limb and inversed dynamics model integrated with inertial measurement unit to calculate motion information, which could ensure good reliability for measurement by the acquisition method. Gao et al. [17] constructed the dynamic model of the seven-bar mechanism of the lower limb exoskeleton rehabilitation robot and simulated it, and the trajectory showed that the exoskeleton system had a good comfort and flexibility in walking training. Guatibonza et al. [18] proposed an auxiliary device of passive rehabilitation training for knee joints and compared the joint trajectory with the experimental trajectory by establishing the kinematics and dynamics models, and the results showed that the auxiliary device had a good effect.

In summary, the current research on lower limb rehabilitation training mainly focuses on the performance analysis and gait trajectory planning of rehabilitation robots under passive training. Compared with passive training, the main advantage of active training is that it can improve patient's active participation and mobilize patient's enthusiasm and self-confidence. At the same time, active training can also carry out individualized treatment according to the specific situation of patients to make the rehabilitation effect more significant, and the recovery in the later stage of rehabilitation accounts for the main part. However, there are few studies on the actual movement of lower limbs in active training, and the actual movement law of lower limbs in the rehabilitation training process is very important to analyze the actual law of limb movement, improve the rehabilitation effect and optimize the training program [19, 20]. Shao et al. [21] measured the joint angle and angular velocity motion data through the lower limb rehabilitation training simulation and compared with the actual measured lower limb motion data during normal walking, which verified the reliability of the lower limb rehabilitation training simulation. Ma et al. [22] studied the law of lower limb movement during rehabilitation training through isokinetic muscle strength training. By comparing the rehabilitation robot before and after training, it was found that the joint angular velocity became larger after robot training, which proved that the rehabilitation robot improved the training effect. Therefore, active rehabilitation training of lower limbs is of great significance to the rehabilitation of patients [23–25].

Aiming at the lack of reference for the law of limb movement in active rehabilitation of lower limbs, the characteristics of limb movement in active training of lower limbs based on five-bar mechanism of man-machine integration system are studied. On the basis of integrating the lower limb and rehabilitation prototype into a human-machine integration system and equivalent to a five-bar mechanism, the forward and inverse kinematics are solved by the D-H method, and then, the five-bar mechanism is constructed by using the solved human physiological joint angle constraint relationship of the hip joint, knee joint

and ankle joint. Lagrange dynamic equation and simulation model analyze the change rules of angle, angular velocity and angular acceleration of hip joint and knee joint at different active training speeds of lower limbs. The joint angle experimental system was built, and 6 representative subjects were selected to actively train the hip and knee joint angle data, which was then substituted into the kinematics model to obtain the lower limb workspace and verify the correctness of the model. The correctness of the simulation is verified by comparing the experimental and simulation data, and a personalized training planning method suitable for people with different lower limb sizes is proposed in order to provide a better rehabilitation effect for lower limb active training.

The main research contents of this paper are as follows: In section 2, a five-bar mechanism is constructed for the man-machine integration system of lower limbs and rehabilitation prototypes. In section 3, based on the D-H method, the forward and inverse kinematics of the system are solved. In the section 4, the Lagrange dynamic equation and simulation model are established to obtain the reasonable speed range of lower limb active rehabilitation training. In the section 5, the experimental system is built to carry out the multi-person joint angle experiment. Based on the error analysis, the human-machine distance planning method is proposed, and the feasibility of the method is verified by comparative analysis. Finally, the conclusions are summarized.

## 2. Establishment of the man-machine integration model

Various forms of movement and speed of human lower limbs, such as flexion, extension and rotation, are transmitted from the hip to the foot in turn, forming complex joint movements that are difficult to simulate by conventional models. Therefore, according to the theory of human anatomy, it is equivalent and split, and the human body is constructed into three mutually perpendicular surfaces and axes, and the lower limbs are divided into thighs, calves and feet with hip joints, knee joints and ankle joints [26]. The hip joint can make the thigh rotate around three axes, internal and external rotation and varus and valgus; the knee joint can make the calf flexion and extension and internal and external rotation relative to the thigh; the ankle joint achieves foot flexion and extension, internal and external rotation, and varus and valgus.

In this paper, the multi-rigid-body system dynamics method is used to divide the lower limbs into several sub-modules according to the structural and functional characteristics of the human body, and the homogeneous rigid body link is defined to connect each sub-module. The equivalent lower limb model is a seven-link model including four spherical joints and two revolute joints, as shown in Fig. 1.

In order to meet the body size of the most people, the representative P5 or P95 percentile size is used as the basis of limb parameters. In this paper, on the basis of selecting the P95 percentile size of the 18 ~ 60 age group of “Chinese adult human body size, the size of each link of the lower limb rigid body mechanism is determined by the size correction method and considering the assembly error [27, 28], as shown in Table I.

In this paper, the lower limb and rehabilitation prototype are integrated into a man-machine integrated system for lower limb active training research. Due to the symmetrical characteristics of the human body structure, the right side of the lower limb is selected as an example for analysis. During active training, the lower limbs actively exert their force, and the legs and feet rotate around the ankle joint, and the feet are connected to the pedal of the rehabilitation prototype. Therefore, the man-machine integration model of the lower limb and the rehabilitation prototype is equivalent to a five-bar mechanism [29], as shown in Fig. 2.

## 3. Forward and inverse kinematics analysis of the five-bar mechanism of man-machine integration system based on D-H method

### 3.1. Kinematics positive solution calculation

Based on the D-H method, the coordinate system of the five-bar mechanism of the man-machine integration system is established. The thigh is defined as the link 1, and the other parts are recursively recursive,

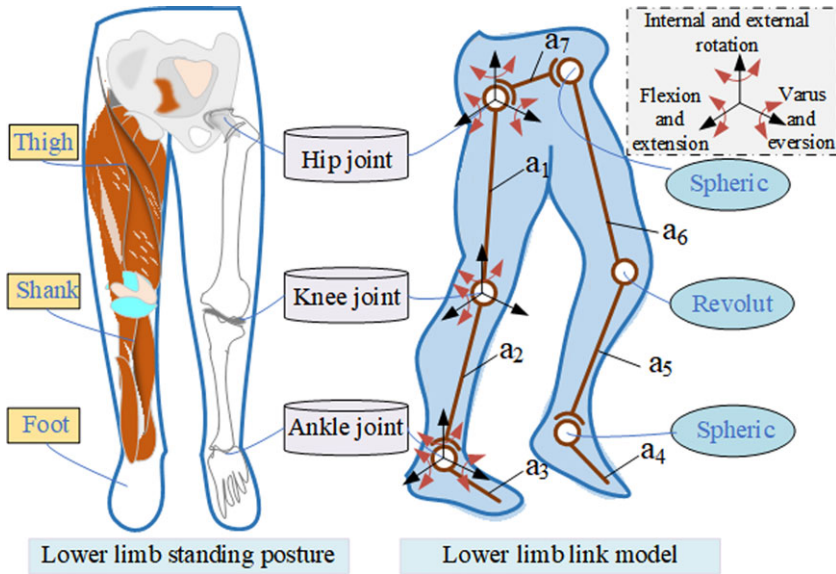


Figure 1. Seven-link model of human lower limb.

as shown in Fig. 3. The hip joint flexion as  $\theta_1$  and it is between the link  $i$  and the horizontal direction, the knee joint extension as  $\theta_2$  and the ankle joint extension as  $\theta_3$ , and the foot handle rotation extension as  $\theta_4$  thanks to the angle between the link  $i-1$  and the link  $i$  extension line. The angle between the rehabilitation prototype shaft and the foot is defined as  $\theta_4$  called the angle of the foot handle, and the angle between the prototype shaft and the frame is defined as  $\theta_5$  called the rotation angle of the prototype.  $\alpha_{i-1}$  is the angle between the link  $i-1$  and the link  $i$  along the  $z$ -axis direction  $x$ -axis,  $d_i$  is the distance between the link  $i-1$  and the link  $i$  along the  $z$ -axis direction. The D-H parameters of Table II are obtained and the forward and inverse kinematics analysis is carried out.

According to the parameters in Table II, the transformation matrices  ${}^0_1T, {}^1_2T, {}^2_3T, {}^3_4T, {}^4_5T$  of each coordinate system are obtained, and they are substituted into the terminal pose matrix to obtain the positive kinematics solution as follows.

$${}^0_5T = {}^0_1T \cdot {}^1_2T \cdot {}^2_3T \cdot {}^3_4T \cdot {}^4_5T = \begin{bmatrix} n_x & o_x & a_x & p_x \\ n_y & o_y & a_y & p_y \\ n_z & o_z & a_z & p_z \\ 0 & 0 & 0 & 1 \end{bmatrix} \tag{1}$$

In the Eq. (1)

$$\begin{aligned} n_x &= \cos(\theta_1 + \theta_2 + \theta_3 + \theta_4 + \theta_5) \\ n_y &= \sin(\theta_1 + \theta_2 + \theta_3 + \theta_4 + \theta_5) \\ n_z &= 0 \\ o_x &= -\sin(\theta_1 + \theta_2 + \theta_3 + \theta_4 + \theta_5) \\ o_y &= \cos(\theta_1 + \theta_2 + \theta_3 + \theta_4 + \theta_5) \\ o_z &= 0 \\ a_x &= 0 \end{aligned}$$

**Table I.** P95 percentile adult male corrected size.

	Thigh	Shank	Foot
Quality (kg)	10.59	3.38	0.977
Length (mm)	480	393	131
Centroid (mm)	240	146.5	65.5
Lower extremity length (mm)	1063		

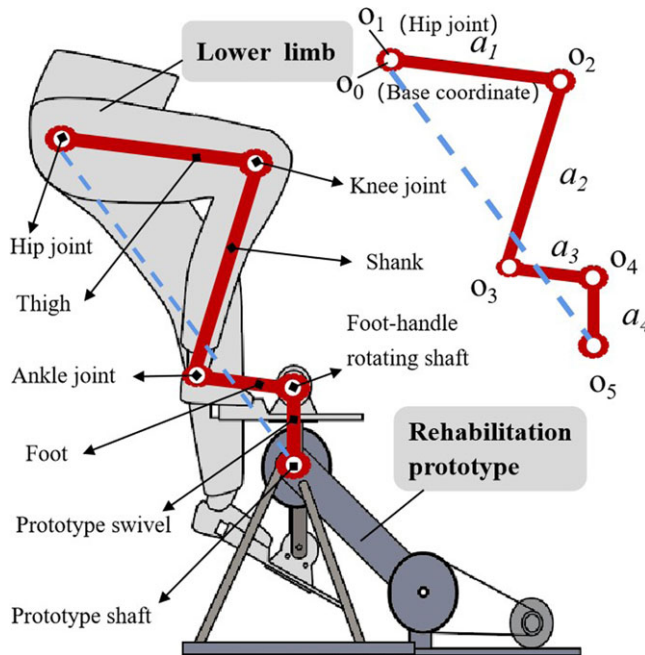


**Figure 2.** Man-machine integration model of active training in lower limb.

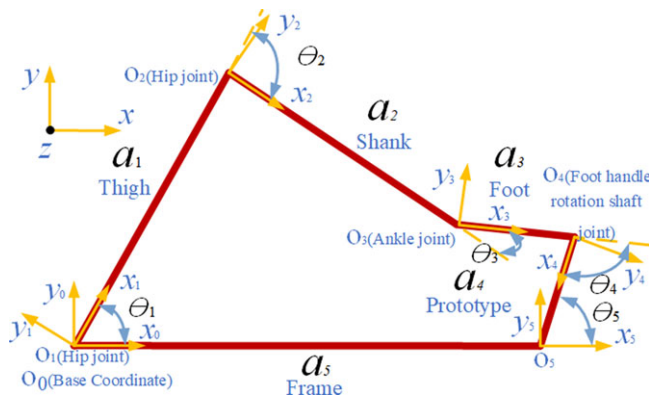


**Figure 3.** D-H coordinate system of the man-machine integrated system for lower limb active training.

**Table II.** D-H parameter table of the man-machine integrated system for lower limb active training.

Link i-1	Link i	$a_{i-1}$ (mm)	$\alpha$ (°)	$d_i$ (mm)	(°)
0	1	$a_1$	0	$d_1$	1
1	2	$a_2$	0	$d_2$	2
2	3	$a_3$	0	$d_3$	3
3	4	$a_4$	0	$d_4$	4
4	5	$a_5$	0	$d_5$	5

$$a_y = 0$$

$$a_z = 1$$

$$p_x = a_4 \cos(\theta_1 + \theta_2 + \theta_3 + \theta_4) = 1$$

$$p_y = a_4 \sin(\theta_1 + \theta_2 + \theta_3 + \theta_4) + a_2 \cos(\theta_1 + \theta_2) + a_1 \sin(\theta_1 + \theta_2) + a_1 \sin \theta_1 + a_3 \sin(\theta_1 + \theta_2 + \theta_3)$$

$$p_z = d_1 + d_2 + d_3 + d_4 + d_5 \tag{2}$$

Through the inverse kinematics calculation of the lower limb active training based on the five-bar mechanism of the man-machine integration system, the expression of each joint angle is obtained, which lays a theoretical foundation for the human-computer interaction of the lower limb active rehabilitation training.

### 3.2. Inverse kinematics solution calculation

Inverse kinematics based on pose parameters is known. Multiplied by  ${}^0T^{-1}$  both sides of the Eq. (1) to the left respectively, that is  ${}^0T^{-1}{}^1T = {}^1T_2{}^2T_3{}^3T_4{}^4T_5$ . The equality [1, 1], [1, 2], [2, 1] and [2, 2] of the matrix elements are equal on both sides respectively, which can get

$$\begin{cases} n_x \cos \theta_1 + n_y \sin \theta_1 = o_y \cos \theta_1 - o_x \sin \theta_1 \\ n_y \cos \theta_1 - n_x \sin \theta_1 = -o_x \cos \theta_1 - o_y \sin \theta_1 \end{cases} \tag{3}$$

From Eq. (3)

$$\theta_1 = \arctan 2(n_y + o_x, n_x - o_y) \tag{4}$$

Multiplied by  ${}^1T^{-1}{}^2T$  on both sides of the Equation sign of Eq. (1) to the left at the same time and take [1, 3] and [2, 3] to be Equation respectively to get

$$\theta_2 = \arctan 2(a_y, a_x) - \arctan 2(n_x - o_y, -o_x - n_y) \tag{5}$$

Taking [1, 4] and [2, 4] in Eq. (1) to corresponding Equation can be obtained

$$2k_1 a_3 \cos(\theta_1 + \theta_2 + \theta_3) + 2k_2 a_3 \sin(\theta_1 + \theta_2 + \theta_3) = k_1^2 + k_2^2 + a_3^2 - a_4^2 \tag{6}$$

In the Eq. (6)

$$\begin{cases} k_1 = p_x - a_2 \cos(\theta_1 + \theta_2) - a_1 \cos \theta_1 \\ k_2 = p_y - a_2 \sin(\theta_1 + \theta_2) - a_1 \sin \theta_1^* \end{cases} \tag{7}$$

$$\begin{cases} a_4 \cos(\theta_1 + \theta_2 + \theta_3 + \theta_4) = p_x - a_2 \cos(\theta_1 + \theta_2) - a_1 \cos \theta_1 - a_3 \cos(\theta_1 + \theta_2 + \theta_3) \\ a_4 \sin(\theta_1 + \theta_2 + \theta_3 + \theta_4) = p_y - a_2 \sin(\theta_1 + \theta_2) - a_1 \sin \theta_1 - a_3 \sin(\theta_1 + \theta_2 + \theta_3) \end{cases} \tag{8}$$

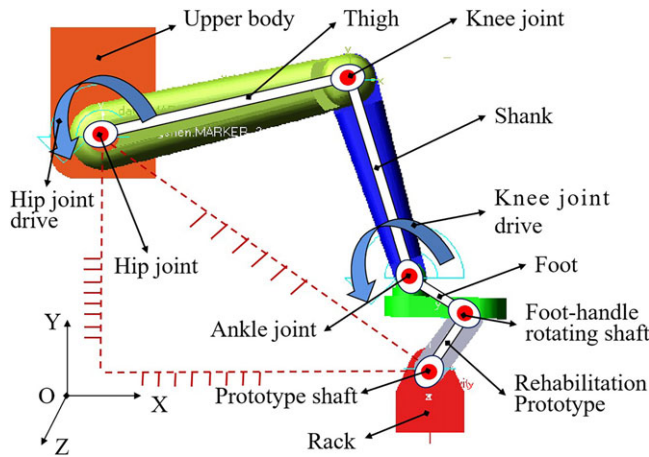


Figure 4. Dynamic coordinate system and simulation of three-dimensional model.

By the simultaneous solution of Eq. (6) and Eq. (8)

$$\theta_3 = \arctan 2\left( A \pm \sqrt{A^2 + B^2 - C^2}, B - C \right) - \arctan 2(a_y, a_x) \tag{9}$$

In the Eq. (9)

$$\begin{cases} A = 2k_2a_3 \\ B = 2k_1a_3 \\ C = k_1^2 + k_2^2 + a_3^2 - a_4^2 \end{cases} \tag{10}$$

$$\theta_4 = \arctan 2(\dot{p}_y - \dot{a}_2 \sin(\theta_1 + \theta_2) - \dot{a}_1 \sin \theta_1 - \dot{a}_3 \sin(\theta_1 + \theta_2 + \theta_3), \dot{p}_x - \dot{a}_2 \cos(\theta_1 + \theta_2) - \dot{a}_1 c\theta_1 - \dot{a}_3 \cos(\theta_1 + \theta_2 + \theta_3) - \arctan 2\left( A \pm \sqrt{A^2 + B^2 - C^2}, B - C \right) \tag{11}$$

Taking [1, 1], [1, 2], [2, 1] and [2, 2] in Eq. (1) to be Equation respectively, then

$$\theta_3 = \arctan 2\left( A \pm \sqrt{A^2 + B^2 - C^2}, B - C \right) - \arctan 2(a_y, a_x) \tag{12}$$

The inverse kinematics solution of active training of lower limb based on the five-bar mechanism of the man-machine integration system is calculated and the expression of each joint angle is obtained, which lays a theoretical foundation for human-computer interaction in lower limb active rehabilitation training.

#### 4. Dynamics modeling and simulation of lower limb active training

##### 4.1. Establishment the dynamics model based on Lagrange method

###### (1) Establish Lagrange coordinate system

The dynamic coordinate system and simulation of three-dimensional model of man-machine system under active training of lower limbs is established, as shown in Fig. 4, the base coordinate system is established at the hip joint position. The thigh, calf, foot and prototype shaft are named as link 1, link 2, link 3 and link 4, respectively. The connection between the hip joint and the base coordinate system is link 5, and the lengths of links 1~5 are  $a_1, a_2, a_3$  and  $a_4$ .

###### (2) Solving the system's kinetic energy

The dynamic Equation of the system is established on the basis of Lagrange function. The Lagrange function is obtained by the differences between the kinetic energy and potential energy of the system, and the kinetic energy and potential energy of the system are superimposed by the kinetic energy and potential energy of each link. Therefore, according to the geometric size relationship of each link in Fig. 3, the coordinates of each particle are described, as shown in the Eq. (13).

$$\begin{cases} x_1 = a_1 \cos \theta_1 / 2 \\ y_1 = a_1 \sin \theta_1 / 2, z_1 = 0 \\ x_2 = a_1 \cos \theta_1 + a_2 \sin(\theta_1 - \theta_2) / 2 \\ y_2 = a_1 \sin \theta_1 - a_2 \cos(\theta_1 - \theta_2) / 2, z_2 = 0 \\ x_3 = a_1 \cos \theta_1 + a_2 \sin(\theta_1 - \theta_2) + a_3 \cos(\theta_1 + \theta_3 - \theta_2) / 2 \\ y_3 = a_1 \sin \theta_1 - a_2 \cos(\theta_1 - \theta_2) - a_3 \sin(\theta_1 + \theta_3 - \theta_2) / 2, z_3 = 0 \\ x_4 = a_1 \cos \theta_1 + a_2 \sin(\theta_1 - \theta_2) + a_3 \cos(\theta_1 + \theta_3 - \theta_2) + a_4 \cos(\theta_1 + \theta_3 - \theta_2 - \theta_4) / 2 \\ y_4 = a_1 \sin \theta_1 - a_2 \cos(\theta_1 - \theta_2) - a_3 \sin(\theta_1 + \theta_3 - \theta_2) - a_4 \sin(\theta_1 + \theta_3 - \theta_2 - \theta_4) / 2, z_4 = 0 \end{cases} \tag{13}$$

In the Eq. (13),  $x$  and  $y$  are the coordinates of the center of mass, all of  $z$  are 0.

The velocity multiplier can be obtained by adding the multipliers of the first derivative of the  $x$ ,  $y$  and  $z$  coordinates of the particle. After obtaining the  $v^2$  of the four particles, the kinetic energy of the link is solved by Eq. (16). Finally, the total kinetic energy of the system can be obtained by superimposing the kinetic energy of four particles, as shown in Eq. (17) and Eq. (18).

$$v_i^2 = \dot{x}_i^2 + \dot{y}_i^2 + \dot{z}_i^2 \tag{14}$$

$$\begin{cases} v_1^2 = \dot{a}_1^2 / 2 \\ v_2^2 = 2\dot{a}_1^2 + \dot{a}_2^2 / 2 - \dot{a}_1 \dot{a}_2 \sin \theta_2 \\ v_3^2 = \dot{a}_1^2 + \dot{a}_2^2 + \dot{a}_3^2 / 4 - 2\dot{a}_1 \dot{a}_2 \sin \theta_2 + \dot{a}_1 \dot{a}_3 \cos(2\theta_1 + \theta_3 - \theta_2) + \dot{a}_2 \dot{a}_3 \sin(2\theta_1 + \theta_3 - 2\theta_2) \\ v_4^2 = \dot{a}_1^2 + \dot{a}_2^2 + \dot{a}_3^2 + \dot{a}_4^2 / 4 - 2\dot{a}_1 \dot{a}_2 \sin \theta_2 + 2\dot{a}_1 \dot{a}_3 \cos(2\theta_1 + \theta_3 - \theta_2) + 2\dot{a}_2 \dot{a}_3 \sin(2\theta_1 + \theta_3 - 2\theta_2) + \\ \quad + \dot{a}_1 \dot{a}_4 \cos(2\theta_1 + \theta_3 - \theta_2 - \theta_4) + \dot{a}_3 \dot{a}_4 \cos \theta_4 + \dot{a}_2 \dot{a}_4 \cos(2\theta_1 + \theta_3 - 2\theta_2 - \theta_4) \end{cases} \tag{15}$$

$$E_{ki} = m_i v_i^2 / 2 \tag{16}$$

$$\begin{cases} E_{k1} = m_1 v_1^2 / 2 = m_1 \dot{a}_1^2 / 4 \\ E_{k2} = m_2 v_2^2 / 2 = m_2 (2\dot{a}_1^2 + \dot{a}_2^2 / 2 - \dot{a}_1 \dot{a}_2 \sin \theta_2) / 2 \\ E_{k3} = m_3 v_3^2 / 2 = m_3 (\dot{a}_1^2 + \dot{a}_2^2 + \dot{a}_3^2 / 4 - 2\dot{a}_1 \dot{a}_2 \sin \theta_2 + \dot{a}_1 \dot{a}_3 \cos(2\theta_1 + \theta_3 - \theta_2) + \\ \quad + \dot{a}_2 \dot{a}_3 \sin(2\theta_1 + \theta_3 - 2\theta_2)) / 2 \\ E_{k4} = m_4 v_4^2 / 2 = m_4 (\dot{a}_1^2 + \dot{a}_2^2 + \dot{a}_3^2 + \dot{a}_4^2 / 4 - 2\dot{a}_1 \dot{a}_2 \sin \theta_2 + 2\dot{a}_1 \dot{a}_3 \cos(2\theta_1 + \theta_3 - \theta_2) + \\ \quad + 2\dot{a}_2 \dot{a}_3 \sin(2\theta_1 + \theta_3 - 2\theta_2) + \dot{a}_1 \dot{a}_4 \cos(2\theta_1 + \theta_3 - \theta_2 - \theta_4) + \dot{a}_3 \dot{a}_4 \cos \theta_4 + \\ \quad + \dot{a}_2 \dot{a}_4 \cos(2\theta_1 + \theta_3 - 2\theta_2 - \theta_4)) / 2 \end{cases} \tag{17}$$

$$E_k = \sum_1^4 E_{ki} = E_{k1} + E_{k2} + E_{k3} + E_{k4} \tag{18}$$

where  $v_i^2 (i = 1, 2, 3, 4)$  are the velocity of the center of mass,  $E_{ki}^2 (i = 1, 2, 3, 4)$  are the kinetic energy of the center of mass,  $m_i^2 (i = 1, 2, 3, 4)$  are the mass of each link,  $E_k$  is the total kinetic energy.



(3) Solving the system potential energy

The potential energy of each particle of the man-machine system is solved by the Eq. (19), and the system potential energy is further superimposed, such as the Eq. (20) and Eq. (21).

$$E_{pi} = m_i g y_i \tag{19}$$

$$\begin{cases} E_{p1} = m_1 g y_1 = m_1 g a_1 \sin \theta_1 / 2 \\ E_{p2} = m_2 g y_2 = m_2 g (a_1 \sin \theta_1 - a_2 \cos(\theta_1 - \theta_2) / 2) \\ E_{p3} = m_3 g y_3 = m_3 g (a_1 \sin \theta_1 - a_2 \cos(\theta_1 - \theta_2) - a_3 \sin(\theta_1 + \theta_3 - \theta_2) / 2) \\ E_{p4} = m_4 g y_4 = m_4 g (a_1 \sin \theta_1 - a_2 \cos(\theta_1 - \theta_2) - a_3 \sin(\theta_1 + \theta_3 - \theta_2) - \\ - a_4 \sin(\theta_1 + \theta_3 - \theta_2 - \theta_4) / 2 \end{cases} \tag{20}$$

$$E_p = \sum_{i=1}^4 E_{pi} = E_{p1} + E_{p2} + E_{p3} + E_{p4} \tag{21}$$

where  $E_{pi}^2 (i = 1, 2, 3, 4)$  are the potential energy of the center of mass,  $E_p$  is the total potential energy.

(4) Establishment of kinetic Equation

The Lagrange function is obtained by the differences between the kinetic energy and the potential energy of the system. The Lagrange function is calculated as shown in the Eq. (25), and the dynamic Equation of the center of mass of the foot can be obtained. It can be observed in the form of matrix Equation, which is composed of inertial force term and gravity term.

$$L = E_k - E_p \tag{22}$$

$$F_i = \frac{d}{dt} \frac{\partial L}{\partial \dot{a}_i} - \frac{\partial L}{\partial a_i} \tag{23}$$

$$\begin{cases} F_1 = (m_1/2 + m_2(2 + \dot{a}_2 \sin \theta_2/2) + m_3(1 + \dot{a}_2 \sin \theta_2 + \dot{a}_3 \cos(2\theta_1 + \theta_3 - \theta_2) / 2) + \\ + m_4 (1 + \dot{a}_2 \sin \theta_2 + \dot{a}_3 \cos(2\theta_1 + \theta_3 - \theta_2) + \dot{a}_4 \cos(2\theta_1 + \theta_3 - \theta_2 - \theta_4) / 2)) a_1^2 - \\ - (m_1 - m_2 - m_3 - m_4) g \sin \theta_1 / 2 \\ F_2 = (m_2(1/2 - \dot{a}_1 \sin \theta_2/2) + m_3(1 - \dot{a}_1 \sin \theta_2 + \dot{a}_3 \sin(2\theta_1 + \theta_3 - 2\theta_2) / 2) + \\ + m_4 (1 + a_1 \sin \theta_2 + a_3 \sin(2\theta_1 + \theta_3 - 2\theta_2) + a_4 \cos(2\theta_1 + \theta_3 - 2\theta_2 - \theta_4) / 2)) \dot{a}_2^2 - \\ - (-m_2 - m_3 - m_4) g \cos(\theta_1 - \theta_2) / 2 \\ F_3 = (m_3(1/4 + a_1 \cos(2\theta_1 + \theta_3 - \theta_2) / 2 + a_2 \sin(2\theta_1 + \theta_3 - 2\theta_2) / 2) + \\ + m_4(1 + a_1 \cos(2\theta_1 + \theta_3 - \theta_2) + \dot{a}_2 \sin(2\theta_1 + \theta_3 - 2\theta_2) + \dot{a}_4 \cos \theta_4) / 2) a_3^2 - \\ - (-m_3 - m_4) g \sin(\theta_1 + \theta_3 - \theta_2) / 2 \\ F_4 = (m_4(1/4 + a_1 \cos(2\theta_1 + \theta_3 - \theta_2 - \theta_4) / 2 + \dot{a}_3 \cos \theta_4 / 2) + \\ + a_2 \cos(2\theta_1 + \theta_3 - 2\theta_2 - \theta_4) / 2) a_4^2 - (-m_4) g \sin(\theta_1 + \theta_3 - \theta_2 - \theta_4) / 2 \end{cases} \tag{24}$$

**Table III.** Body size and key information of the six subjects.

Parts	Parameter	Value
Upper body and the rehabilitation prototype frame	Density (g/cm <sup>3</sup> )	7.80
	Young's modulus (MPa)	2.07 × 10 <sup>5</sup>
	Poisson's ratio	0.29
	Materials	carbon steel
Thigh, calf, foot and prototype shaft	Density (g/cm <sup>3</sup> )	2.74
	Young's modulus (MPa)	7.17 × 10 <sup>4</sup>
	Poisson's ratio	0.33
	Materials	Aluminum alloys

$$F_i = \begin{bmatrix} F_1 \\ F_2 \\ F_3 \\ F_4 \end{bmatrix} = \begin{bmatrix} G_1 & 0 & 0 & 0 \\ 0 & G_2 & 0 & 0 \\ 0 & 0 & G_3 & 0 \\ 0 & 0 & 0 & G_4 \end{bmatrix} \begin{bmatrix} \ddot{a}_1^2 \\ a_2^2 \\ \ddot{a}_3^2 \\ \ddot{a}_4^2 \end{bmatrix} + \begin{bmatrix} (m_1 - m_2 - m_3 - m_4) \sin \theta_1 \\ (-m_2 - m_3 - m_4) \cos(\theta_1 - \theta_2) \\ (-m_3 - m_4) \sin(\theta_1 + \theta_3 - \theta_2) \\ (-m_4) \sin(\theta_1 + \theta_3 - \theta_2 - \theta_4) \end{bmatrix} g/2 \quad (25)$$

$$G_1 = ((m_1/2 + 2m_2 + m_3 + m_4) + (m_2/2 + m_3 + m_4) \dot{a}_2 \sin \theta_2 + (m_3/2 + m_4) \dot{a}_3 \cos(2\theta_1 + \theta_3 - \theta_2) + (m_4/2) a_4 \cos(2\theta_1 + \theta_3 - \theta_2 - \theta_4))$$

$$G_2 = (m_2/2 + m_3 + m_4) + (-m_2/2 - m_3 + m_4) \dot{a}_1 \sin \theta_2 + (m_3/2 + m_4) \dot{a}_3 \sin(2\theta_1 + \theta_3 - 2\theta_2) + (m_4/2) \dot{a}_4 \cos(2\theta_1 + \theta_3 - 2\theta_2 - \theta_4)$$

$$G_3 = (m_3/4 + m_4) + (m_3/2 + m_4) a_1 \cos(2\theta_1 + \theta_3 - \theta_2) + (m_3/2 + m_4) a_2 \sin(2\theta_1 + \theta_3 - 2\theta_2) + (m_4/2) \dot{a}_4 \cos \theta_4$$

$$G_4 = m_4/4 + m_4 \dot{a}_1 \cos(2\theta_1 + \theta_3 - \theta_2 - \theta_4) / 2 + (m_4/2) \dot{a}_2 \cos(2\theta_1 + \theta_3 - 2\theta_2 - \theta_4) + (m_4/2) \dot{a}_3 \cos \theta_4 \quad (26)$$

**4.2. Establishment of the dynamic simulation model**

In order to further analyze the motion law of hip joint, knee joint and ankle joint in active training of lower limbs, and verify the correctness of theoretical derivation of dynamic model, the dynamic simulation model of five-bar mechanism of man-machine integration system is established in ADAMS environment of 2019 version of MAS company in the United States, as shown in Fig. 4. According to the data in Table III, the model size is set. The length of link of the prototype is 131 mm, the dynamic simulation parameters are shown in Table III. Fixed constraints are set on the upper body and the rehabilitation prototype to ensure that the positions of the two are unchanged, and rotation constraints are added to each joint to ensure that each joint can rotate relatively.

The joint angle associated motion constraint setting plays a key role in the simulation under multi-joint angle uncertainty. In this paper, based on human physiology and the coordinate system of Fig. 3, the constraint relationship among hip joint, knee joint and ankle joint is obtained for the first time by analytical method, such as Eq. (27) and Eq. (28), so as to realize the constraint setting of each joint in the dynamic simulation model. According to Fig. 4, Since the five-bar mechanism of the man-machine integration system has two degrees of freedom, a rotation drive is added to the corresponding revolute joints of the hip joint and the ankle joint.

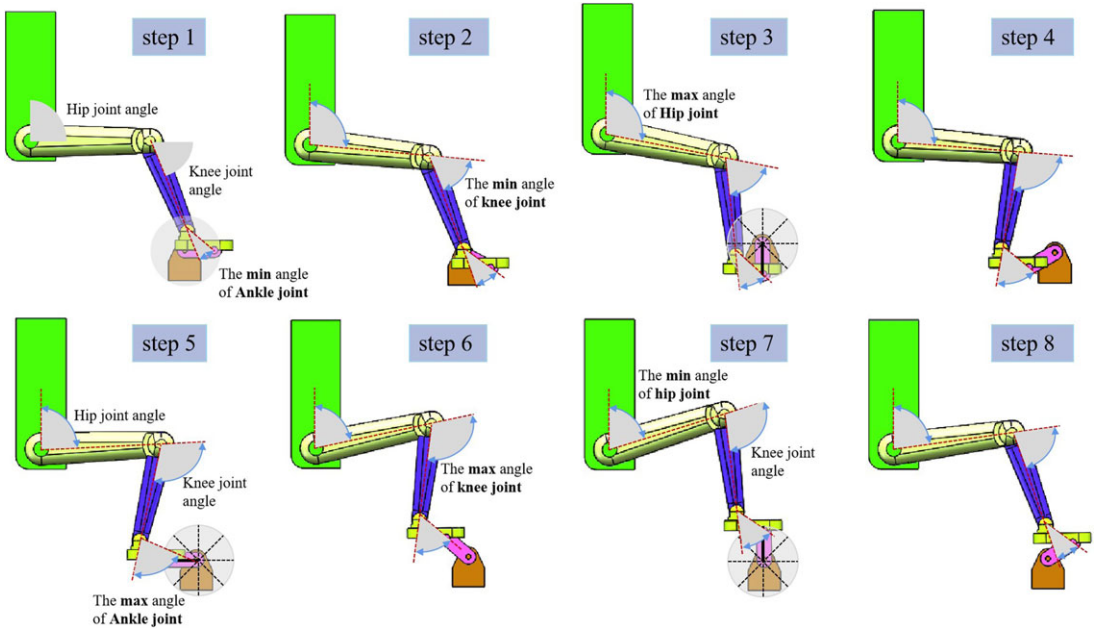


Figure 5. The steps of active rehabilitation training of lower limbs.

In order to make the thigh movement stable, the hip joint is driven by sinusoidal speed [30]. At the same time, the simulation speed should be close to the actual lower limb rehabilitation training speed, so the speed is set to  $n_1 = 10 / \Delta t \sin(2\pi t/5)$  and the direction is counterclockwise. According to the constraint relationship between hip joint, knee joint and ankle joint, the motion correlation curve is created [31], according to the hip joint speed through the CUBSPL function in ADAMS environment and then the ankle joint speed is set to  $n_2 = \text{CUBSPL}(t, 0, \text{SPLINE}, 0)^\circ/\text{s}$  and the direction is counterclockwise. In addition, a single flexion and extension cycle time is set to 5 s, and the number of steps is 50. The simulated measurement angles of the hip, knee joint and ankle joints are the horizontal angle between thigh and  $x$ -axis, the angle between thigh and calf, and the angle between calf and foot, the steps of active rehabilitation training of lower limbs are shown in Fig. 5.

$$\begin{cases} a_1 \sin \theta_1 + a_2 \sin(\theta_2 - \theta_1) - a_3 \sin(\theta_2 - \theta_1 - \theta_3) - a_4 \sin \theta_4 = 0 \\ a_1 \cos \theta_1 + a_2 \cos(\theta_2 - \theta_1) - a_3 \cos(\theta_2 - \theta_1 - \theta_3) - a_4 \cos \theta_4 - a_5 = 0 \end{cases} \quad (27)$$

$$a_2 \cos(\theta_2 - \theta_1) = a_4 \cos \theta_4 + a_3 \cos(\theta_2 - \theta_1 - \theta_3) - a_1 \cos \theta_1 \quad (28)$$

Figure 5 shows the movement steps of lower limb rehabilitation training in a single cycle. In the first half of the cycle, the ankle joint angle is the smallest, then the knee joint angle is the smallest, and then the hip joint angle is the largest. The appearance of the three angles shows a certain lag law. In the second half of the cycle, the law shows the opposite trend.

By simulating that the angle changes curves of hip joint, knee joint and ankle joint are obtained. In order to make the results convenient for analysis, each angle is transformed into the angle between lower limb and vertical direction, and the angle change law of three joints in a single flexion and extension cycle is obtained, as shown in Fig. 6. It can be observed that the angle range of hip joint flexion and extension are  $80.02^\circ \sim 99.98^\circ$ , and the angle range of knee joint flexion and extension are  $62.62^\circ \sim 109.05^\circ$ . The angle range of ankle joint flexion and extension is  $51.24^\circ \sim 101.47^\circ$ .

The results show that the motion amplitude of the hip joint is the smallest, the motion amplitude of the knee joint and the ankle joint is larger and the peak angle shows a stable lag change compared with

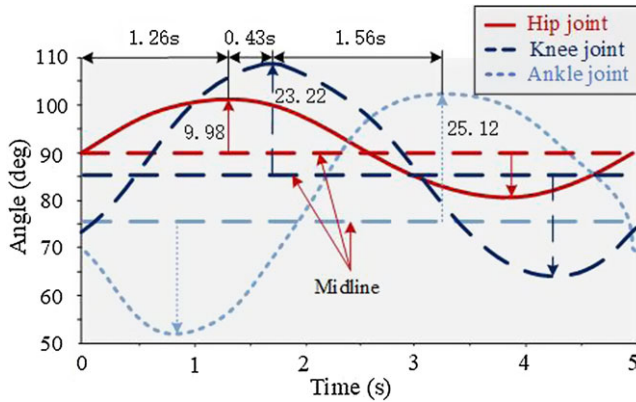


Figure 6. Angle changes of the hip, knee and ankle joints.

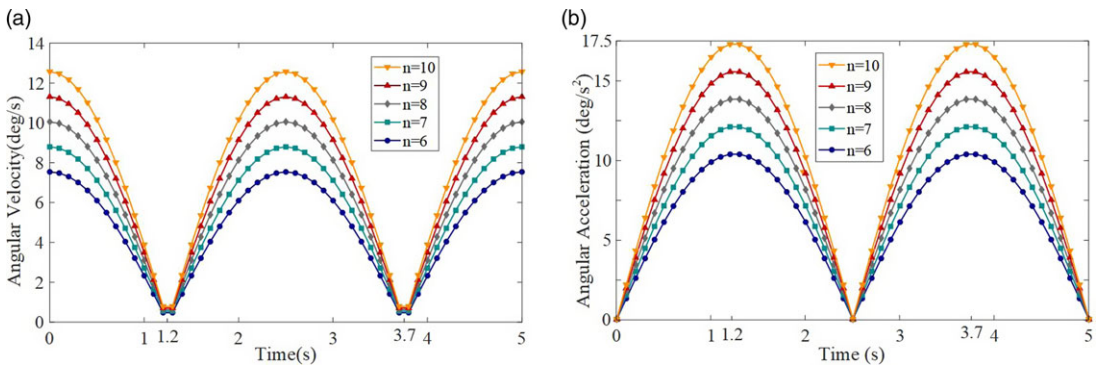


Figure 7. Hip joint angular velocity and angular acceleration curve. (a) Hip joint angular velocity curve; (b) Hip joint angular acceleration curve.

the motion law of the hip joint, but the change rules of the two are similar. The angle change curve of each angle is continuous and smooth transition, and the angle change range of the three joints is within a reasonable range, which is in line with the active training of lower limbs.

At the same time, considering that the knee joint is more vulnerable to injury than the ankle joint in actual activities [32, 33], and the ankle joint bears most of the body’s gravity in daily actions, so the joint rehabilitation is clinically suitable for resting and drug treatment, so this paper further selects the hip joint and knee joint to analyze the movement law in lower limb rehabilitation training.

### 4.3. Simulation of different active training speeds of lower limbs

In order to analyze the influence of different speed training on the rehabilitation [34], the sine speed  $N = n / \Delta t \sin(2\pi t/5)^\circ/s$  with different amplitude is further used to simulate the effect of rehabilitation training at different speeds. The selected speed is close to the actual rehabilitation training requirements to obtain more accurate rehabilitation rules. It is found that the angle, angular velocity and angular acceleration peak value and extreme point of both hip and knee joints change with “n,” but the change rule is basically unchanged.

From Fig. 7, it can be seen that the angular velocity and angular acceleration of the hip joint increase with the increase of the rotational speed, and the speed is consistent at the limit position of 1.2 s and 3.7 s, but at this time, the acceleration is positively correlated with the rotational speed, and the curve gradually appears sharp points with the increase of the rotational speed. Therefore, the rotational speed

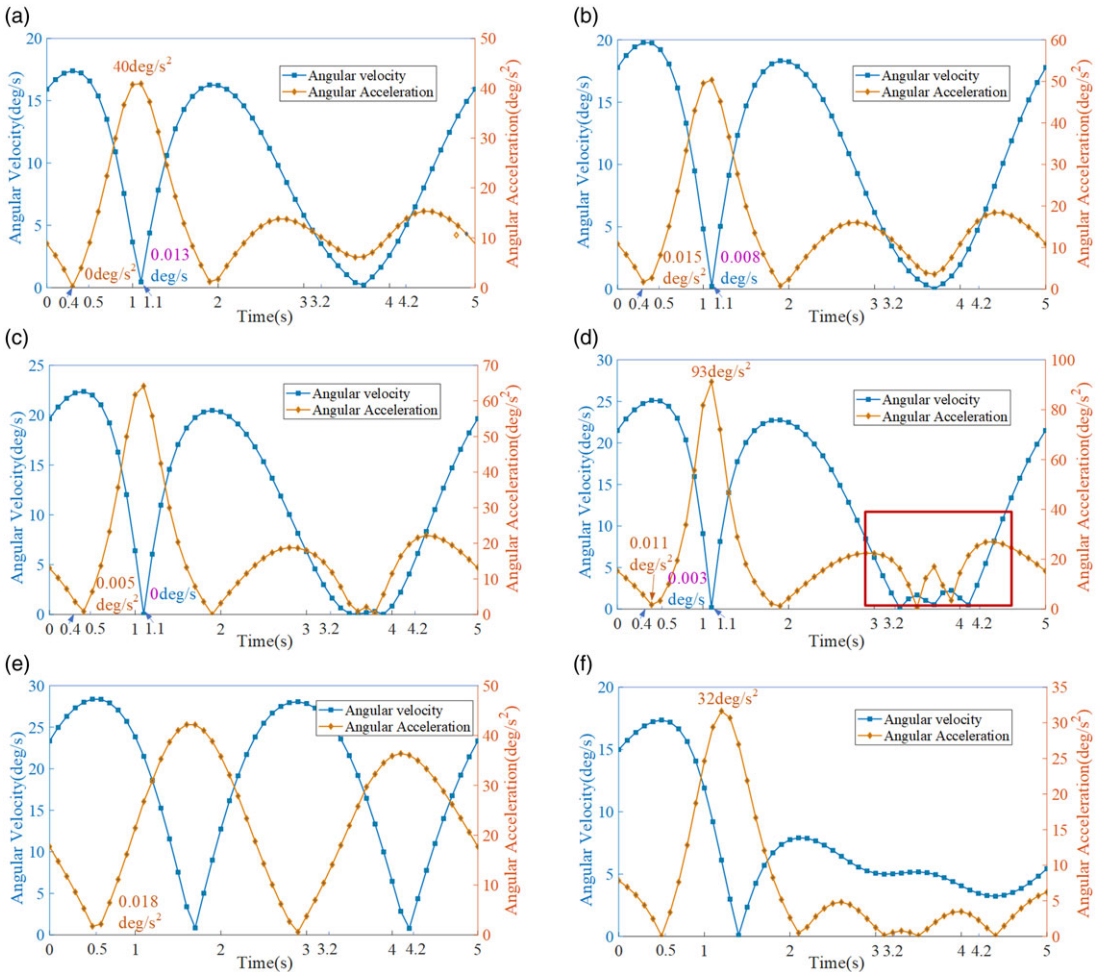


**Figure 8.** Angular velocity and acceleration curves of hip joints at a different velocity. (a)  $n = 6$ ; (b)  $n = 7$ ; (c)  $n = 8$ ; (d)  $n = 9$ ; (e)  $n = 10$ ; (f)  $n = 11$ .

needs to be controlled within a reasonable range to reduce the secondary damage to the lower limbs caused by the impact of the limit position.

By obtaining the knee joint angular velocity and angular acceleration curves, as shown in Fig. 8, the reasonable velocity range is further analyzed.

Figure 8 shows the angular velocity of the knee joint at different speeds showed similar changes. When the speed  $n$  is in the range of 6~7, the angular acceleration increases from 0 to  $0.015^\circ/s^2$  and then decreases to  $0.005^\circ/s^2$  at 0.4~0.5s at the startup moment. Therefore, the acceleration fluctuation is the smallest at the speed  $n = 7$ , and the secondary damage can be avoided by extending the startup time. The angular velocity was reduced from 0.013 to 0 at 1.1 s, indicating that the rehabilitation training action was smoother when  $n < 7$ . The angular acceleration increased from  $40^\circ/s^2$  to  $93^\circ/s^2$  in the range of  $n = 6 \sim 9$ , and gradually decreased to  $32^\circ/s^2$  in the range of  $n = 9 \sim 11$ . The smaller the maximum angular acceleration, the smoother the rehabilitation action. In the 3.2~4.2 s time period, the angular acceleration of the speed  $n = 8 \sim 11$  fluctuates many times, while the angular velocity  $n = 6 \sim 8$  is smooth and excessive, and there is no sudden change in the acceleration when  $n = 6 \sim 7$ . Therefore, in order to reduce the secondary injury of the lower limbs caused by the acceleration mutation, the hip joint speed of no more than  $7/t^* \sin(2*\Pi/5)^\circ/s$  should be selected for lower limb active rehabilitation training to achieve better results.

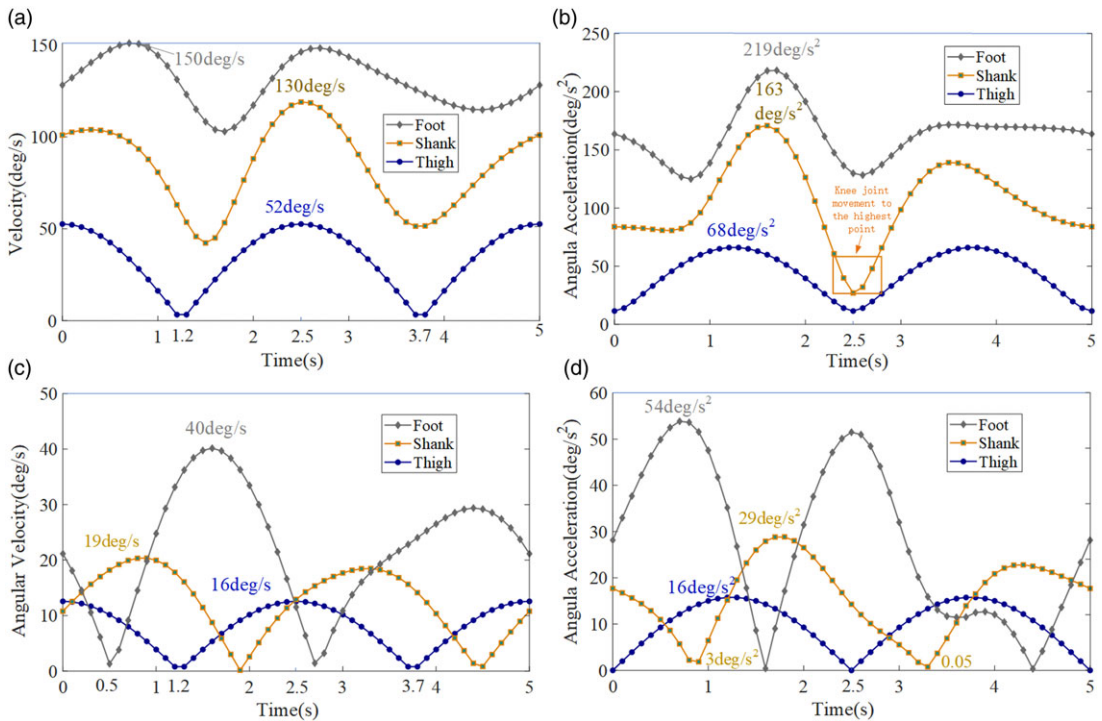


**Figure 9.** The motion law of thigh, calf and foot. (a) Velocity curves; (b) Acceleration curves; (c) Angular velocity curves; (d) Angular acceleration curves.

In order to verify the feasibility of the selected reasonable speed, the speed and acceleration can reflect the speed of the lower limb movement, while the angular velocity and angular acceleration reflect the speed of the lower limb rotation, and then analyze the motion characteristics of the lower limb at multiple levels. The speed, acceleration, angular velocity and angular acceleration of the thigh, calf and foot at  $N = 7 / \Delta t \sin(2\pi t/5)^\circ/s$  are comprehensively analyzed, and the speed and acceleration curves are obtained as shown in Fig. 9.

It can be seen from Fig. 9(a) and Fig. 9(b) that the speed changes of thigh, calf and foot are similar, and there is no sudden change point. The delay of movement from thigh to foot is consistent with the actual movement law, indicating that the simulation method is correct. At the same time, the maximum velocity of thigh, calf and foot is 52 °/s, 130 °/s and 150 °/s, respectively, and the acceleration is 68 °/s<sup>2</sup>, 163 °/s<sup>2</sup> and 219 °/s<sup>2</sup>, respectively. At 2.5s, the acceleration of the calf fluctuates. At this time, the knee joint moves to the highest position in the rehabilitation training. Therefore, at this time, the secondary injury can be reduced by slowing the movement. It can be seen from Fig. 9(c) and Fig. 9(d) that the angular velocity and angular acceleration curves of thigh, calf and foot are smooth, indicating that they move smoothly. However, the angular velocity of the calf rotates at 0.5 s without obvious fluctuation, so that it will not cause secondary damage to the rehabilitation training. The maximum angular acceleration is 54 °/s<sup>2</sup>, and there is no obvious fluctuation in the whole cycle. Therefore, there is no sudden change in speed and angular acceleration, indicating that the active training of lower limbs based on the selected speed meets the requirements, which proves the feasibility of the speed.

## 5. Joint angle experiment and result analysis

### 5.1. Joint angle experiment

The hip and knee joint angles were measured by the joint angle experimental system shown in Fig. 10.

The BWT61CL type attitude sensor with an accuracy of 0.05° angle produced by Shenzhen Weite

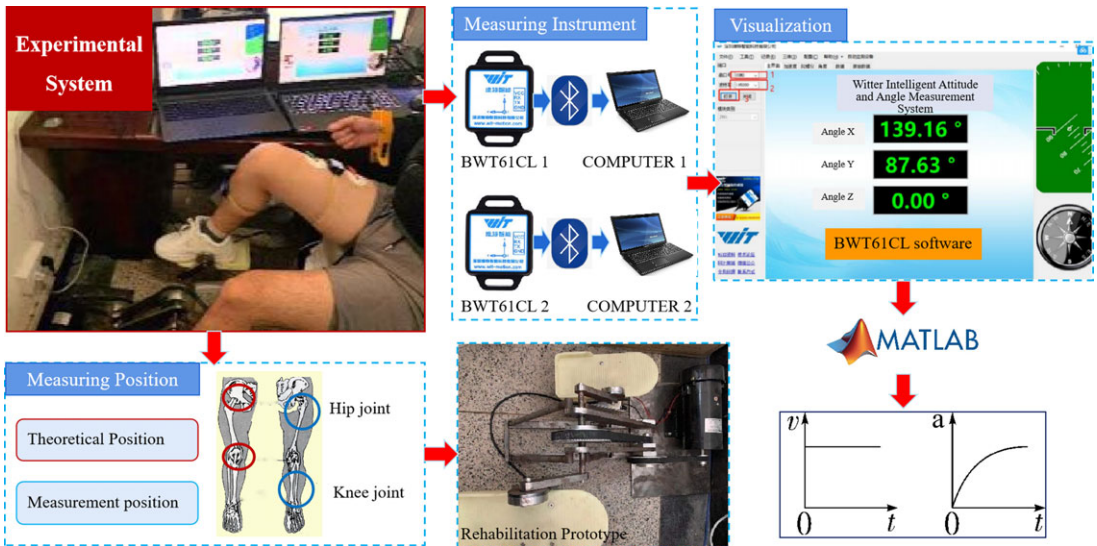


Figure 10. Joint angle experimental system.

Intelligent Company is selected to collect the joint angle, and the sensor is connected to the computer and the initial parameter setting is carried out through Bluetooth. In the experiment, the sensor was placed near the joint position to measure the corresponding angle [35].

The subject's feet were placed at the rotating shaft of the prototype, and the initial position was kept at the level of the thighs, and then the legs simultaneously exerted force to rotate the prototype's rotating shaft in the same direction. In order to reduce the experimental error caused by the individual differences of different subjects, all subjects maintained an unified sitting posture during the experiment. Through the pre-experiment, the data of the same training duration were recorded after the lower limbs were kept at a constant speed. Each subject repeated three experiments for a total of 60 sets of data. The dynamic simulation model was established by measuring the size of each subject's lower limb, and the angles of hip joint and knee joint were obtained by the same simulation method in sections 3.1. The angle was compared with the experimental angle to obtain more accurate lower limb motion characteristics.

In this experiment, 20 subjects (10 males and 10 females) were recruited, who were graduate students of Beijing University of Information Science and Technology ( $170\pm 8$  cm in height,  $67\pm 8$  kg in weight,  $25\pm 2$  years old), the body size and key information were shown in Table IV, and the corresponding body mass index (BMI) was measured. BMI is calculated by dividing weight (Kg) by the square of height (m). It is currently widely used to measure the degree of body fatness, the different body types of people to be taken into account so as to eliminate the influence of personal factors. without skeletal and limb motor dysfunction. They were familiar with the experimental process and in good mental condition during the experiment. They volunteered to experiment and signed the informed consent of the experiment.

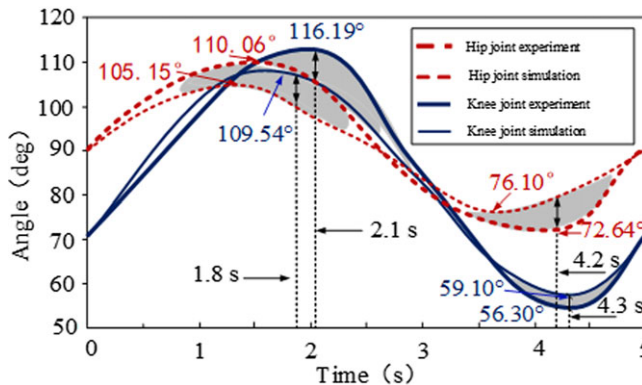
### 5.2. Results and discussion

The angles of the hip and knee joints measured by the active training experiment of a single subject in a flexion and extension cycle were compared with the dynamic simulation results, as shown in Fig. 11.

It can be seen from Fig. 11 that the maximum angles of hip joint experiment and simulation are  $110.06^\circ$  and  $105.15^\circ$  respectively, and the minimum angles are  $72.64^\circ$  and  $76.10^\circ$ , respectively. The maximum angles of knee joint experiment and simulation were  $116.19^\circ$  and  $109.54^\circ$ , respectively, and the minimum angles were  $56.30^\circ$  and  $59.10^\circ$ , respectively. The results show that the experimental and simulation joint angles have the same trend, and the experimental and simulation angles are within the

**Table IV.** *Body size and key information of the six subjects.*

Number	Age	Height (cm)	Weight (kg)	BMI (height/weight)	Thigh (mm)	Shank (mm)
1	26	167	54	19.4	480	390
2	25	170	65	22.5	480	393
3	26	174	65	21.5	500	410
4	24	175	64	20.9	480	400
5	28	184	76	22.4	556	476
6	24	190	77	21.3	550	480

**Figure 11.** *Comparison of hip and knee joint experiments and simulation angles under active training.*

reasonable range of human joint motion. The maximum and minimum angles appear at the highest and lowest points of joint movement in rehabilitation training, respectively. At this time, the maximum experimental and simulation errors also indicate that the lower limb movement to this position should be slowed down. The angular range of motion of the hip joint and knee joint experiment is greater than that of the simulation. The reason is that the inertia of the subject causes the prototype shaft to disengage from the limb when it is in a vertical position, and this phenomenon will become more obvious as the speed increases.

Through simulation, the joint motion law under the actual rehabilitation training conditions is obtained, and the secondary damage caused by the impact is reduced. Further comparison with the experimental results is carried out, and the errors and causes are analyzed to improve the effectiveness of rehabilitation training. The maximum error of the hip joint appears at 1.8 s and 4.2 s, and the knee joint is at 2.1 s and 4.3 s, both of which appear near the limit position of the joint angle, corresponding to the highest and lowest positions of the rehabilitation prototype shaft in the foot during active training. The maximum error of the hip joint is 9.84%, and the maximum error of the knee joint is 4.51%, both within the allowable range of 15%, which were within the allowable range of 15% error verified in Reference [36, 37], meeting the needs of rehabilitation training.

In order to obtain a more accurate joint angle change rule of lower limb active training, the experimental data of 20 subjects were further processed, and the corresponding body mass index (BMI) was measured. BMI is calculated by dividing weight (Kg) by the square of height (m). It is currently widely used to measure the degree of body fatness, so as to take into account the different body types of people and eliminate the influence of personal factors. Due to the close height, the lower limb movement rules are similar. Therefore, a total of 18 groups of representative 6 subjects were selected with height as the reference object. In order to make the experimental data more analytical and accurate, the same experimental method is used to control the same range of hip joint activity of all subjects. Setting the range of hip joint activity can reduce the secondary injury caused by the excessive range of hip joint activity and



**Table V.** Simulation and experimental data of lower limb active training of six subjects.

Subject number	The range of hip joint angle(°)		Error	The range of knee joint angle(°)		Error
	Simulation	Experiment	$ \delta_{max} $	Simulation	Experiment	$ \delta_{max} $
1	80.02 ~ 99.98	78.25 ~ 112.26	7.25%	70.54 ~ 109.01	76.35 ~ 110.86	1.70%
2	80.02 ~ 99.98	72.44 ~ 110.19	9.84%	62.62 ~ 109.05	56.30 ~ 113.97	4.51%
3	80.02 ~ 99.98	74.54 ~ 109.52	8.20%	72.33 ~ 110.80	76.31 ~ 104.38	5.79%
4	80.02 ~ 99.98	76.32 ~ 108.54	6.59%	67.14 ~ 105.61	79.61 ~ 102.37	3.07%
5	80.02 ~ 99.98	81.34 ~ 102.59	2.13%	71.24 ~ 109.71	83.57 ~ 103.15	5.60%
6	80.02 ~ 99.98	80.25 ~ 104.39	2.35%	70.91 ~ 110.38	81.64 ~ 101.36	8.17%

simulate the actual movement law of different groups of people under the same active training, so as to obtain a personalized rehabilitation training program. Therefore, the range of motion of the joint angle is obtained and the maximum error absolute values( $|\delta_{max}|$ ) of the maximum and minimum joint angles of the simulation and experiment are analyzed respectively. The simulation and experimental data of the lower limb active training of 6 subjects are obtained, as shown in Table V.

From the data in Table V, it can be seen that under the same training speed and man-machine distance, the simulated hip joint angle range of motion is consistent, and the knee joint angle range of motion varies with height, weight and BMI. The larger the size of the lower limbs, the smaller the experimental angle range of the hip joint and the knee joint, and the smaller the error of the hip joint. The knee joint is the opposite, indicating that the hip joint training is better than the knee joint to maintain a smaller distance between the human and the machine, while the knee joint is the opposite. The maximum range of hip and knee joint angles of the subjects were  $72.44^\circ \sim 110.19^\circ$  and  $56.30^\circ \sim 113.97^\circ$ , respectively, which were within the allowable range. The error range of hip joint is 2.13% ~ 9.84%, and the error range of knee joint is 1.70% ~ 8.17%, both of which are less than 10%, which meets the experimental requirements.

In summary, the experimental hip and knee joint angles are consistent with the simulation angle, and the errors are within the allowable range. The reasons are as follows: (1) The human body size and training speed of the experiment and simulation cannot be exactly the same, and the experiment is influenced by limb inertia; (2) During the experiment, the vibration of the lower limbs caused the measurement data of the attitude angle sensor to be too large; (3) In the simulation, the lower limb movement is a relatively simple plane motion, while in the experiment, the lower limb has a complex spatial motion, which cannot be simulated.

Combining the errors of the hip and the knee joint, the angle of the hip and the knee joint measured by the subject 4 experiment was substituted into the 2.1 kinematics model to obtain the overall working space of the lower limb, as shown in Fig. 12.

It can be seen that the working space of the lower limb is a ring with an outer ring radius of 612 mm in the  $xoy$  plane, and its inner diameter of 130 mm is close to the length of the rehabilitation prototype shaft. The width of the ring corresponds to the sum of the length of the calf and the foot. Therefore, the simulation workspace verifies the theoretical calculation in Section 3.1 and conforms to the actual situation, indicating that the kinematic model is correct, which provides a theoretical reference for the design and gait planning of lower limb rehabilitation robots.

Under the same speed and man-machine distance, the lower limb movements of subjects with different BMI, height or weight are different. Through the analysis of this difference, the personalized training rules of different lower limb sizes are explored. Therefore, the relationship between the subjects with different BMI and the range of motion of the joint angle is obtained, as shown in Fig. 13.

From Fig. 13, it can be seen that the range of hip joint angle changes of subjects with different BMI is basically the same, which reflects that the change of hip joint is mainly affected by training speed. At the same time, it can be seen that under the same training speed and man-machine distance, the angle of hip joint and knee joint is the largest at the same time when BMI is 22.5, but the angle of hip joint

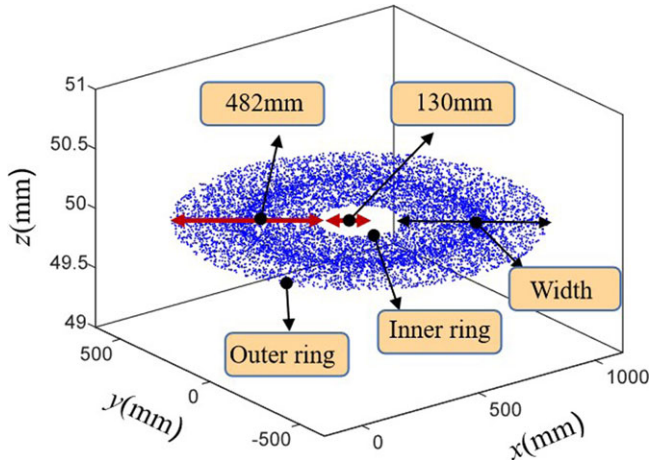


Figure 12. Workspace of lower limb in active training.

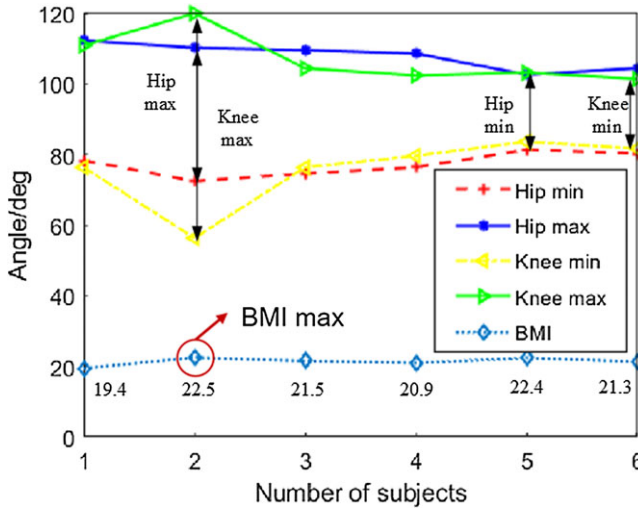
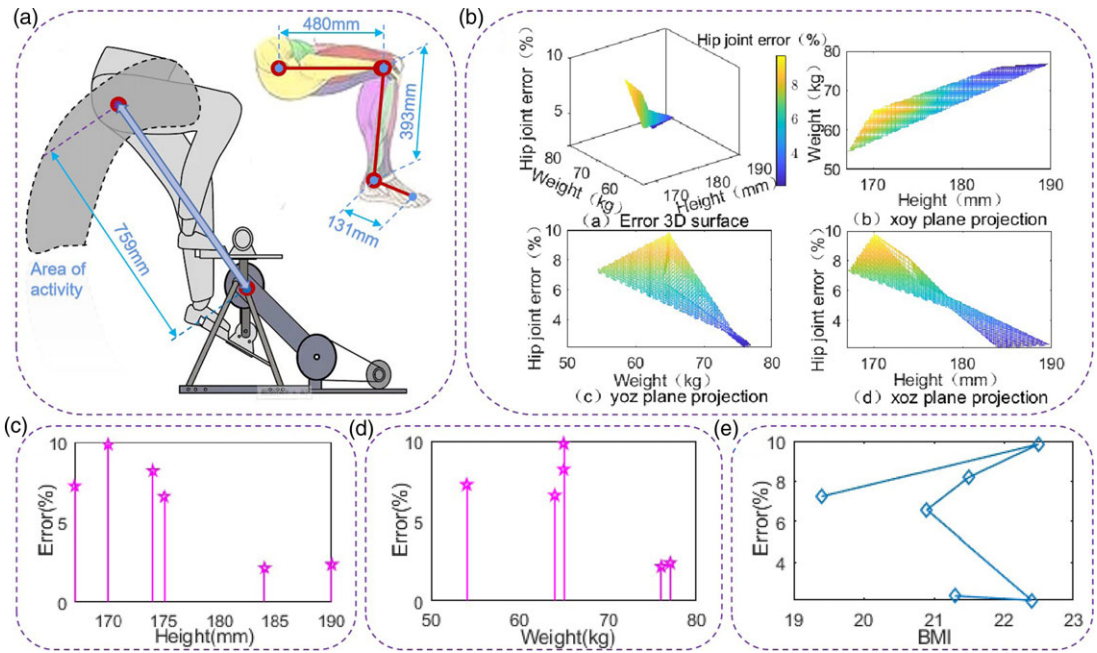


Figure 13. The range of joint motion in subjects with different BMI.

is the smallest at 22.4, and the knee joint is the smallest at 21.3, indicating that the change of hip joint angle has little effect with BMI, while the change of knee joint angle has significant effect.

The relationship between the angle error of the hip joint and the knee joint and the height and weight is shown in Fig. 14 and Fig. 15 respectively.

From Fig. 14(a) and (b) and Fig. 15(a) and (b), it can be seen that the angle error of hip joint experiment and simulation decreases with the increase in body height and weight. The angle error of knee joint experiment and simulation increases with the increase in height and weight. It can be seen from Fig. 14(c)–(e) and Fig. 15(c)–(e) that the error of hip joint and knee joint is closer to the change rule of height, and the error is also different under the same BMI, indicating that the height which is proportional to the size of the lower limb is the main factor of error, and the weight is the secondary factor. At the same time, according to Section 3.2, it is found that the angle of joint activity decreases with the decrease of training speed. Due to the same man-machine distance, the higher the height, the larger the lower limb size, the smaller the distance between the hip joint and the knee joint and the center of



**Figure 14.** Relationship between hip joint angle error and height and weight. (a) Man-machine distance diagram. (b) Relationship between hip angle error and body weight. (c) Relationship between error and height. (d) Relationship between error and weight. (e) Relationship between error and BMI.

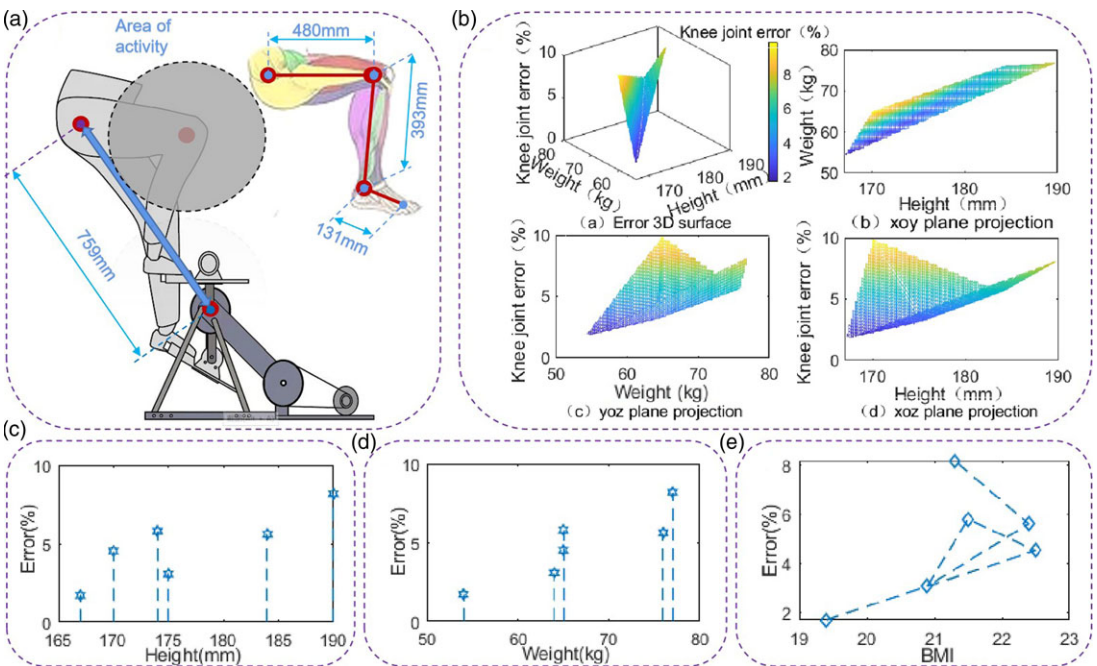


**Figure 15.** Relationship between knee joint angle error and height and weight. (a) Man-machine distance diagram. (b) Relationship between knee angle error and body weight. (c) Relationship between error and height. (d) Relationship between error and weight. (e) Relationship between error and BMI.

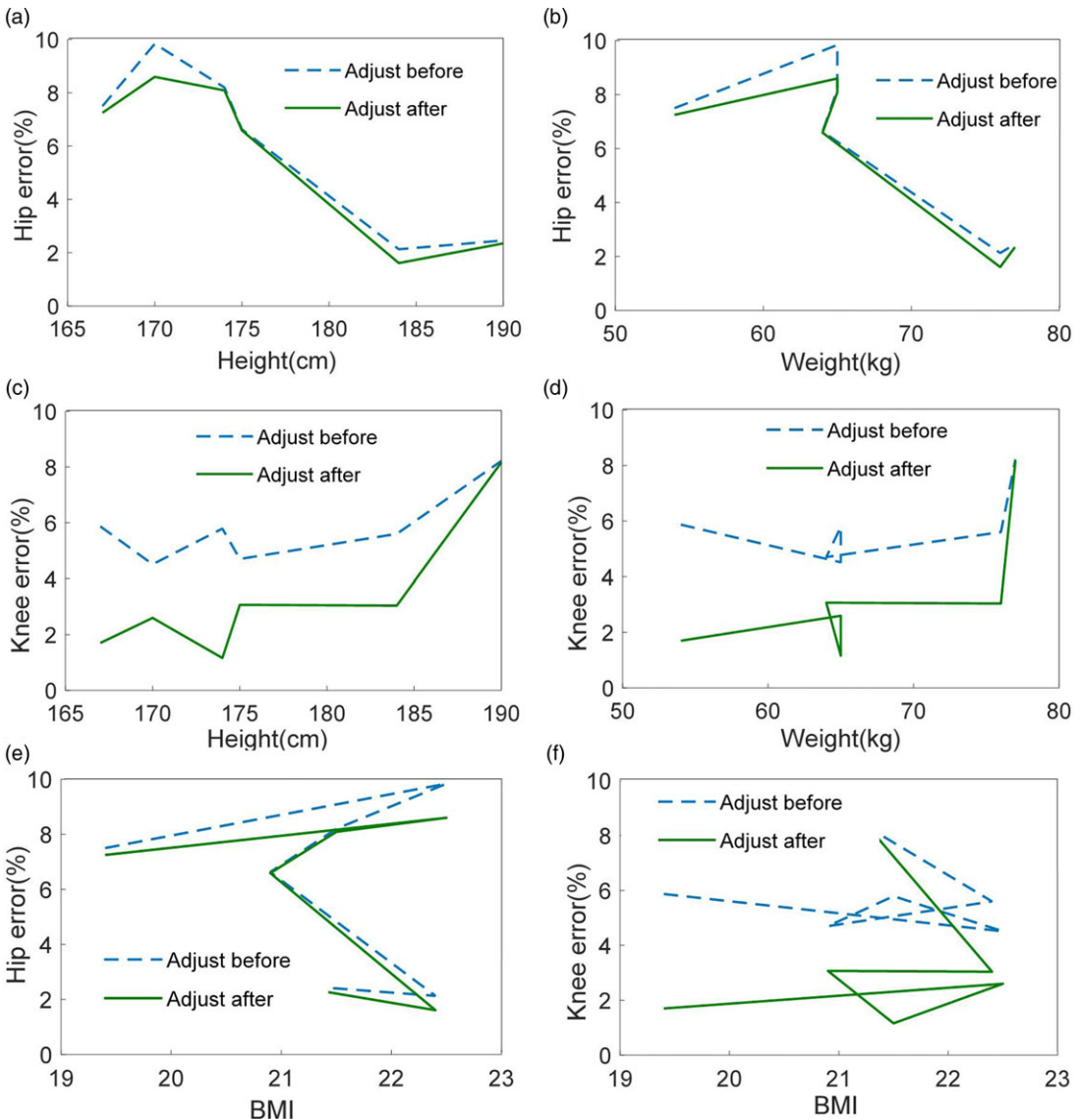


**Figure 16.** Comparison of joint errors before and after adjustment. (a) Height-hip error; (b) Weight-hip error; (c) Height-knee error; (d) Weight-knee error; (e) BMI-hip error; (f) BMI-knee error.

the rehabilitation prototype shaft, indicating that the smaller the distance, the smaller the hip joint error, and the knee joint is the opposite.

Therefore, for the active training of lower limbs based on hip joint, the smaller the height and weight, the lower the training speed or the smaller the man-machine position distance can be appropriately reduced to obtain a hip joint training range closer to the theory; for knee-based rehabilitation training, the training speed can be appropriately reduced or the man-machine distance can be increased to reduce the error to obtain a range of activity angles closer to the knee joint theory, so as to achieve better training results.

For the hip and knee joints, the above strategies are verified by changing the man-machine distance by taking the 5 cm reduction and increase as examples, and the error effects of height, weight and BMI on the two are obtained respectively, as shown in Fig. 16.

It can be seen from Fig. 16 that with the increase of man-machine distance, the hip joint error decreases with different body height and weight, and the knee joint also has the same effect with the decrease of man-machine distance. The errors of hip joint and knee joint are reduced by 1.2% and 4.6% respectively, and the errors of BMI on hip joint and knee joint are reduced by 1.2% and 4.1% respectively. Therefore, it shows that the accuracy of rehabilitation training can be improved by adjusting the training method of human-machine distance planning. At the same time, the feasibility of the personalized planning method proposed in this paper is verified.

## 6. Conclusion

Aiming at the clinical rehabilitation needs of patients with lower limb movement disorders, this study innovatively integrates the lower limbs and rehabilitation prototype into a five-bar mechanism of man-machine integration system and then studies the active training law of lower limbs. Based on the physiological joint-related movement of the human body, the constraint relationship between the hip joint, knee joint and ankle joint is obtained. The lower limb and rehabilitation prototype are integrated into the man-machine integration system and equivalent to a five-bar mechanism. Based on the D-H method, the forward and inverse kinematics analysis is carried out. The workspace of the lower limb is a ring with an inner diameter of 130 mm and an outer diameter of 612 mm in the xoy plane, which is in line with the actual motion situation and verifies the correctness of the kinematics model. By establishing the Lagrange dynamic equation of the five-bar mechanism of the lower limb man-machine integration system, the expressions of inertial force and gravity influence are obtained. Then the dynamic simulation model is constructed to simulate the hip joint and knee joint at different training speeds. The relationship between the angle error of hip joint and knee joint and height and weight was analyzed respectively. Then, the joint angle experimental system is built to carry out the experiment, and the experimental joint angle is compared with the simulation angle to analyze the causes of the error, so as to formulate the corresponding personalized rehabilitation training planning method. Appropriately reducing the training speed or reducing the man-machine position distance to reduce the error, while knee joint training is the opposite, in order to obtain a range of activity angles closer to the hip joint theory and achieve better rehabilitation effect. By increasing and reducing the horizontal man-machine distance of 5 cm, the error of hip joint and knee joint is reduced compared with that before adjustment, which shows that the effect of rehabilitation training is improved, and the feasibility of adjusting man-machine distance by personalized planning method is verified.

This study creatively solves the simulation problem of the lower limb five-bar mechanism and the rehabilitation prototype man-machine integration system under multi-angle uncertainty in the active training process. Compared with the traditional lower limb rehabilitation training, which only focuses on the study of the motion law of the rehabilitation robot, it makes up for the deficiency of the lower limb rehabilitation training for the study of the motion law of the lower limb. In addition, the obtained human-machine integrated motion characteristics of the lower limb can provide reference value for the optimization of rehabilitation training programs and gait planning.

**Author contributions.** A short statement must be provided indicating how each author contributed to the work. For example, AB and CD conceived and designed the study. CD and EF conducted data gathering. GH performed statistical analyses. AB, EF and GH wrote the article.

**Financial support.** This study was funded by the Foundation for National Major Scientific Instruments Project (Grant No. 2014YQ24044504) and 2019 Industrial Technology Foundation Public Service Platform Project (Grant No. 0714EMTC000898). The authors would like to thank the anonymous referees for their efforts and valuable comments.

**Competing interests.** The author(s) declared no potential competing interests with respect to the research, authorship and/or publication of this article.

**Ethical approval.** The studies involving human participants were reviewed and approved by school. Written informed consent to participate in this study was provided by the participants' legal guardian/next of kin. The animal study was reviewed and

approved by school. Written informed consent was obtained from the minor(s)' legal guardian/next of kin for the publication of any potentially identifiable images or data included in this article. Besides, the experiment of this study is still in the experimental stage, has not yet entered the clinical stage, and all experiments were completed in the laboratory.

## References

- [1] E. Trinnachoke, S. Viboon, "A Lower limb rehabilitation robot in sitting position with a review of training activities," *J Healthc Eng* **2018**, 1927807 (2018).
- [2] China Disabled Persons' Federation, Statistical bulletin on the development of disabled persons in 2019, (2020).
- [3] L.D. Wang, B. Peng and Zhang H. Q., "Summary of "China stroke prevention and treatment report 2020,"" *Chinese J Cerebr Dis* **19**(02), 136–144 (2022).
- [4] S. Bhardwaj, A. A. Khan and M. Muzammil, "Lower limb rehabilitation robotics: The current understanding and technology," *Work* **69**(3), 100–109 (2021).
- [5] C.C. Pang, R. L. Li and Feng Y. P., "Research progress on the application of rehabilitation robots in stroke hemiplegia rehabilitation," *Nurs Res* **33**(21), 3715–3719 (2019).
- [6] X. Liu, M. Yang and Yang M. L., "Application of multi-position intelligent lower limb rehabilitation robot in rehabilitation training of stroke patients," *Biomed Eng Clin* **22**(03), 299–303 (2018).
- [7] B. Guo, J. Han, X. Li, T. Fang and A. You, "Research and design of a new horizontal lower limb rehabilitation training robot," *Int J Adv Robot Syst* **13**(1), 10 (2016).
- [8] I. Carpinella, T. Lencioni, T. Bowman, R. Bertoni, A. Turolla, M. Ferrarin and J. Jonsdottir, "Effects of robot therapy on upper body kinematics and arm function in person post-stroke: A pilot randomized controlled trial," *J NeuroEng Rehabil* **17**(1), 10 (2020).
- [9] J. Zhao, X. Zhou and Yang X. N., "Research of wire-driven parallel lower limb rehabilitation robot," *J Phys: Conf Series* **2229**(1), 28–43 (2022).
- [10] H. Cheng, R. Huang and Qiu J., "A review of rehabilitation robots and their clinical applications," *Robotics* **43**(05), 606–619 (2021).
- [11] Q. Q. Fang, T. Xu and Zheng T. J., "A rehabilitation training interactive method for lower limb exoskeleton robot," *Math Prob Eng* **1**, 10–25 (2022).
- [12] B. Langley, A. Jones, T. Board and M. Greig, "Modified conventional gait model vs. Six degrees of freedom model: A comparison of lower limb kinematics and associated error," *Gait Post* **89**, 1–6 (2021).
- [13] I. Jakob, A. Kollreider, M. Germanotta, F. Benetti, A. Cruciani, L. Padua and I. Aprile, "Robotic and sensor technology for upper limb rehabilitation," *PM&R* **10**(4), 189–197 (2018).
- [14] A. Mohamed, N. Jyotindra and Dwivedy K., "Event-triggered adaptive control for upper-limb robot-assisted passive rehabilitation exercises with input delay," *Proceed Inst Mech Eng* **236**(4), 832–845 (2022).
- [15] H. Wang, M. Lin, Z. Jin, H. Yan, G. Liu, S. Liu and X. Hu, "A 4-DOF workspace lower limb rehabilitation robot: Mechanism design, human joint analysis and trajectory planning," *Appl sci* **10**(13), 4542–4560 (2020).
- [16] W. D. Li, Li J. and Li X., "Dynamics analysis and parameter optimization of underactuated heterogeneous lower limb rehabilitation robots," *J Zhejiang Univ (Eng Sci)* **55**(02), 222–228 (2021).
- [17] Ma J. T., *IMU-based inverse dynamics modeling and power-assisted simulation of lower limb walking* (Harbin Institute of Technology, Harbin, 2019).
- [18] M. Gao, Z. Wang, Z. Pang, J. Sun, J. Li, S. Li and H. Zhang, "Electrically driven lower limb exoskeleton rehabilitation robot based on anthropomorphic design," *Machines* **10**(4), 266–293 (2022).
- [19] A. Guatibonza, L. Solaque and A. Velasco, "Parallel assistive robotic system for knee rehabilitation: Kinematic and dynamic modeling validation," *J Med Eng Technol* **46**(8), 637–647 (2022).
- [20] X. Wang, Y. Feng, J. Zhang, Y. Li, J. Niu, Y. Yang and H. Wang, "Design and analysis of a lower limb rehabilitation training component for bedridden stroke patients," *Machines* **9**(10), 224–239 (2021).
- [21] Z. W. Shao, J. Li and L. T. Yu, "A method for self-service rehabilitation training of human lower limbs," (2022), arXiv preprint [arXiv:2205.08853](https://arxiv.org/abs/2205.08853).
- [22] H. Ma, "Research on Promotion of Lower Limb Movement Function Recovery after Stroke by Using Lower Limb Rehabilitation Robot in Combination with Constant Velocity Muscle Strength Training," **In: 7th International Symposium on Mechatronics and Industrial Informatics (ISMII)**, Zhuhai, China (2021) pp. 70–73.
- [23] D. Quaglia, M. Gasperi, R. Coser, G. Grisenti, M. Scartozzi, E. Girardi and N. Mazzini, "Robotic rehabilitation effect on upper limb recovery in post-acute stroke," *Gait Post* **66**(1), 31–32 (2018).
- [24] P. Comfort, P. A. Jones, L. C. Smith and L. Herrington, "Joint kinetics and kinematics during common lower limb rehabilitation exercises," *J Athl Training* **50**(10), 1011–1018 (2015).
- [25] K. X. Khor, H. A. Rahman, S. K. Fu, L. S. Sim, C. F. Yeong and E. L. M. Su, "A novel hybrid rehabilitation robot for upper and lower limb rehabilitation training," *Procedia Comput Sci* **42**(1), 293–300 (2014).
- [26] L. Pianta, M. Bigoni, V. Cimolin, N. Cau, S. Baudo and A. Mauro, "Does kinematics add meaningful information to clinical assessment in upper limb rehabilitation after stroke," *Gait Post* **42**, 20–21 (2015).
- [27] J. Bai, *Research On Key Technologies and Rehabilitation Evaluation of Upper Limb Rehabilitation Robot* (Southeast University, Nanjing, 2019).
- [28] H. C. Shang, Ji T. and FuX. L., "Structural design and dynamic analysis of lower limb rehabilitation robot," *Mech Des Manufac* **375**(5), 253–256 (2022).

- [29] S. Y. Yan, Y. Q. Xu and Y. Chen. *Ergonomics and Product Design* (Harbin Institute of Technology Press, Harbin, 2017). 20–29.
- [30] L. Meng, C. A. Macleod, B. Porr and H. Gollee, “Bipedal robotic walking control derived from analysis of human locomotion,” *Biol Cybern* **112**(3), 277–290 (2018).
- [31] M. M. Tan and Y. K. Jia, “Kinematics analysis and simulation of hip rehabilitation robot,” *Comp Eng Appl* **7**, 1–9 (2022).
- [32] T. Xia, Q. Huan and Chen Y., “Design and kinematics analysis of lower limb exoskeleton rehabilitation robot,” *J Huaqiao Univ (Nat Sci Edn)* **38**(04), 452–456 (2017).
- [33] E. Shao, Z. Lu, X. Cen, Z. Zheng, D. Sun and Y. Gu, “The effect of fatigue on lower limb joint stiffness at different walking speeds,” *Diagnostics* **12**(6), 1470–1482 (2022).
- [34] M. Bicer, A. T. M. Phillips and L. Modenese, “Altering the strength of the muscles crossing the lower limb joints only affects knee joint reaction forces,” *Gait Post* **95**, 210–216 (2022).
- [35] M. Li, Q. Xue, S. Yang, X. Han and S. Zhang, “Effects analysis of handrail height on sit-to-stand movement under knee joint support in healthy young adults,” *Res Biomed Engi* **38**(2), 617–628 (2022).
- [36] P. A. Ataabadi, J. Sarvestan and Alaei F., “Linear and non-linear analysis of lower limb joints angle variability during running at different speeds,” *Acta Gymnica* **51**, 23–31 (2021).
- [37] B. Khuyagbaatar, T. Purevsuren and D. Ganbat, “Normal range of motion of lower extremity joints in Mongolian subjects,” *Engineering Proceedings* **11**(1), 29–29 (2021).

---

**Cite this article:** J. Sun, F. Hu, K. Gao, F. Gao, C. Ma and J. Wang (2024). “Research and experiment on active training of lower limb based on five-bar mechanism of man-machine integration system”, *Robotica* **42**, 1453–1475. <https://doi.org/10.1017/S0263574724000304>